[1]N. R. Werthamer, Phys. Rev. A 2, 2050 (1970).
[2]N. R. Werthamer, Phys. Rev. 185, 348 (1969).
[3]N. R. Werthamer, R. L. Gray, and T. R. Koehler, Phys. Rev. B 2, 4199 (1970); B 4, 1324 (1971).
[4]R. E. Slusher and C. M. Surko, Phys. Rev. Letters (to be published).
[5]J. Ruvalds, Phys. Rev. B 3, 3556 (1971); J. Ruvalds and A. Zawadowski, *ibid.* B 2, 1172 (1970).
[6]F. Iwamoto, Progr. Theoret. Phys. (Kyoto) 44, 1121 (1970); 44, 1135 (1970); J. Ruvalds and A. Zawadowski, Phys. Rev. Letters 25, 333 (1970); L. P. Pitaevskii, Zh. Eksperim. i Teor. Phys. Pis'ma v Redaktsiyu 12, 118 (1970) [Sov. Phys. JETP Letters 12, 82 (1970)]; A. Zawadowski, J. Ruvalds, and J. Solana, Phys. Rev. A (to be published).
[7]R. A. Cowley and A. D. B. Woods, Can. J. Phys. 49, 177 (1971).
[8]T. J. Greytak, R. Woerner, J. Yan, and R. Benjamin, Phys. Rev. Letters 25, 1547 (1970).
[9]J. Ranninger, Ann. Phys. (N. Y.) 45, 452 (1967); 49, 297 (1968); L. J. Sham, Phys. Rev. 156, 494 (1967); 163, 401 (1967).
[10]N. R. Werthamer, Phys. Rev. B 1, 572 (1970).
[11]H. Horner, Phys. Letters 25A, 464 (1967).
[12]R. A. Cowley and W. J. L. Buyers, J. Phys. C 2, 2262 (1969); R. A. Cowley, E. C. Svensson, and W. J. L. Buyers, Phys. Rev. Letters 23, 525 (1969).

PHYSICAL REVIEW B VOLUME 5, NUMBER 2 15 JANUARY 1972

Electronic Structure of the 3*d* Transition-Metal Monoxides. I. Energy-Band Results

L. F. Mattheiss
Bell Laboratories, Murray Hill, New Jersey 07974
(Received 5 August 1971)

The augmented-plane-wave (APW) method is applied to calculate the nonmagnetic band structures for the 3*d* transition-series monoxides CaO, TiO, VO, MnO, FeO, CoO, and NiO, all of which form with the rocksalt structure. The APW energy-band results at seven symmetry points in the fcc Brillouin zone are fitted with the Slater and Koster linear-combination-of-atomic-orbitals (LCAO) interpolation method involving nonorthogonal orbitals. A nonlinear least-squares fitting procedure is applied to determine 16 two-center energy and overlap LCAO parameters which characterize the oxygen 2*s*-2*p* and transition-metal 3*d* energy bands and their interactions. It is found that both the APW results and the corresponding LCAO parameters exhibit systematic variations across this series of compounds. These calculations predict that: (a) CaO is an insulator with a 10-eV band gap; (b) the metallic oxides TiO and VO have 3*d* bandwidths of about 0.5 Ry, which are two and a half times larger than those for the antiferromagnetic insulators MnO, FeO, CoO, and NiO; (c) the energy of the 3*d* band decreases systematically (relative to the bottom of the transition-metal 4*s*-4*p* band) as the nuclear charge is increased, causing the metal *s*-*d* bands to overlap for the early but not the later members of this series.

I. INTRODUCTION

The electronic properties of the 3*d* transition-metal oxides have been the subject of recent theoretical interest and speculation. This interest has focused mainly on the question of whether the 3*d* electrons in these oxides are in itinerant Bloch or localized Wannier states. The review article by Adler[1] summarizes many of the theoretical models that have been proposed to explain the limited and sometimes contradictory experimental results which are presently available for these compounds.

Among this wide variety of compounds, the simplest from a structural point of view are the 3*d* transition-metal monoxides which form with the rocksalt structure. Unfortunately, this simplicity is not reflected in their physical properties, for these monoxides include materials that are Bloch-Wilson insulators (CaO), ordinary metals (TiO and VO), and antiferromagnetic insulators (MnO, FeO, CoO, and NiO).

The purpose of this investigation is to provide an over-all picture of the one-electron energy-band structures for these 3*d* transition-metal monoxides with the rocksalt structure. Even if such a one-electron picture is not valid for these materials, these results can provide a useful starting point for the theoretical treatment of problems dealing with vacancies, electron-electron interactions, polaron effects, crystal-field effects, and superexchange. The present paper is concerned only with the one-electron energy-band results. The interpretation of these results and their relation to experiment are considered in Paper II.[2]

The present calculations are carried out in two stages. In the initial stage, the nonrelativistic augmented-plane-wave (APW) method is applied to calculate the nonmagnetic band structures for each of the 3*d* transition-metal monoxides CaO, TiO, VO, MnO, FeO, CoO, and NiO. The calculations involve *ad hoc* crystal potentials which are derived from neutral-atom charge densities for the con-

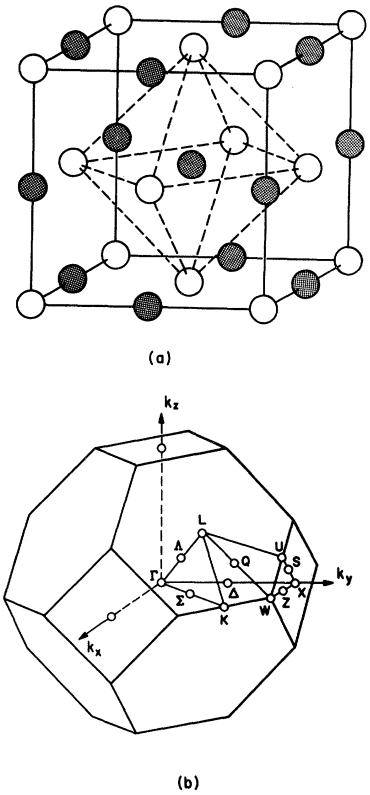

FIG. 1. (a) Cubic unit cell of the rocksalt structure with dashed lines indicating the octahedral coordination of the central metal atom with its six neighboring ligands. (b) Brillouin zone for the fcc bravais lattice.

stituent atoms, using techniques similar to those applied earlier in a band calculation for rhenium trioxide (ReO_3).[3] In these applications of the APW method, the corrections to the muffin-tin potential in the region outside the APW spheres have been treated exactly while the nonspherical terms within the spheres have been neglected. In the present study, the actual APW calculations are limited to seven points of high symmetry in the fcc Brillouin zone.

In the second stage of this investigation, the APW results are fitted with the Slater and Koster[4] linear-combination-of-atomic-orbitals (LCAO) interpolation method. This variation of the LCAO method, which involves nonorthogonal metal and ligand orbitals, has been applied previously to fit the energy bands for ReO_3.[5] Using a nonlinear least-squares fitting procedure, the 49 APW energy eigenvalues at the seven symmetry points have been fitted in order to determine 16 LCAO energy and overlap parameters for each compound (with the exception of CaO, which was not considered). Thirteen of these LCAO parameters represent nearest-neighbor metal-metal, oxygen-oxygen, and metal-oxygen energy interactions involving the metal $3d$ and oxygen $2s$ and $2p$ orbitals. The final three parameters represent $3d$-$2s$ and $3d$-$2p$ orbital overlap effects.

It is found that the accuracy of the LCAO fit to the APW results improves with increasing atomic number of the metal atom. The maximum error in the LCAO fit varies from 0.05 Ry in TiO to 0.01 Ry in NiO. In most cases, the largest errors involve states that hybridize strongly with the metal $4s$-$4p$ bands. It is concluded that these states must be added to the LCAO formalism if increased accuracy is to be achieved. Hybridization between the overlapping calcium $4s$-$4p$ and $3d$ bands prevents a meaningful application of this simplified LCAO model to the CaO energy bands.

This paper is divided into four sections. The details of the present series of calculations are presented in Sec. II. These include a description of the APW and LCAO calculations, a tabulation of the LCAO matrix for the rocksalt structure, and a summary of the nonlinear least-squares method that is used to determine the LCAO parameters. The APW energy-band results and the corresponding LCAO parameters for the entire series of compounds (except CaO) are presented in Sec. III. Finally, Sec. IV contains a discussion of these results and a comparison with those obtained in previous calculations for these oxides with the rocksalt structure.

II. COMPUTATIONAL DETAILS

A. APW Calculations

The rocksalt or sodium-chloride structure consists of two interpenetrating fcc lattices of metal and ligand atoms which are displaced relative to one another by $\frac{1}{2}a$ along $\langle 100 \rangle$, where a is the cubic-cell dimension. As shown in Fig. 1(a), both the metal and the ligand atoms are situated at sites with full cubic (O_h) point symmetry. The dashed lines in Fig. 1(a) indicate the octahedral coordination of a given metal atom by its six neighboring ligands. The Brillouin zone for the fcc bravais lattice is shown in Fig. 1(b), where the standard notation is used to label the various symmetry points and lines. The lattice parameters that are used in the present APW calculations are listed in Table I.

The *ad hoc* crystal potentials involved in this study have been calculated by superimposing the neutral-atom Hartree-Fock-Slater charge densities of Herman and Skillman[6] with the electronic configurations $2p^4$ for the oxygen and $3d^n 4s^1$ for the metal atoms. The detailed numerical techniques have been described previously.[3] These APW calculations include the corrections to the muffin-tin potential in the region outside the APW spheres exactly but neglect the nonspherical corrections within the APW spheres. The values for the various sphere radii R_M and R_0 are listed in Table I. These

TABLE I. Lattice parameters and sphere radii for the transition-metal monoxides MO.

MO	a(Å)	a(a.u.)	R_M(a.u.)	R_0(a.u.)	Ref.
CaO	4.799	9.069	2.442	2.093	a
TiO	4.181	7.901	2.127	1.823	b
VO	4.093	7.735	2.083	1.785	a
MnO	4.435	8.381	2.256	1.934	a
FeO	4.31	8.145	2.193	1.880	c
CoO	4.260	8.051	2.168	1.858	a
NiO	4.195	7.927	2.134	1.829	a

[a]W. B. Pearson, *A Handbook of Lattice Spacings and Structures of Metals and Alloys* (Pergamon, New York, 1958).

[b]A. D. Pearson, J. Phys. Chem. Solids 5, 316 (1958).

[c]J. S. Smart, Phys. Rev. 82, 113 (1951).

radii have been chosen to optimize the convergence of the APW eigenvalues. This is achieved by choosing the individual sphere radii as large as possible, i.e., touching along the ⟨100⟩ directions. To approximately equalize the convergence of both the oxygen $2p$ and the transition-metal $3d$ states, the ratio R_M/R_0 has been set equal to $\frac{7}{6}$. With this choice of sphere radii, the region outside the APW spheres corresponds to 47% of the total unit cell volume and approximately 100 APW basis functions are required to obtain energy eigenvalues that are converged to about 0.001 Ry.

This choice proves to be a sensible one in another respect. In each compound, it is found that these sphere radii consistently fall near the maximum in the potential that occurs along the line joining the metal and oxygen nuclei. As a result, this choice of sphere radii minimizes the corrections to the muffin-tin potential in the regions within as well as outside the APW spheres.

The corrections to the muffin-tin potential outside the APW spheres have a much smaller effect on the enengy bands in the rocksalt structure than they did in previous calculations for ReO_3.[3] This is due to the fact that the rocksalt structure is more closely packed than ReO_3, having 53% rather than 24% of the unit cell inside the APW spheres. It is found that the potential outside the APW spheres in these rocksalt-structured compounds exhibits peak-to-peak variations (relative to the muffin-tin constant) which are as large as 0.8 Ry. These are one-third the size of those calculated in ReO_3 and twice as large as those calculated by DeCicco[7] for KCl. It is found that these muffin-tin corrections shift some energy eigenvalues by as much as a few hundredths of a rydberg, though these shifts are usually found to be much smaller. These shifts are similar in magnitude to those that DeCicco has calculated for KCl, and they represent a substantial reduction from the 0.3-Ry shifts that were calculated for ReO_3.[3]

The use of neutral-atom rather than ionic charge densities to construct the crystal potentials for these compounds is a novel feature of the present calculations since most previous investigations have been based on ionic-type potentials. The virtues of this neutral-atom model are (i) its simplicity; and (ii) the fact that it usually leads to energy-band results that are in reasonable agreement with experiment. Actually, the distinction between the neutral-atom and ionic models is somewhat arbitrary since there is no unique way of assigning the electronic charge within a given unit cell of the crystal to the individual atoms within that cell. Slater[8] has pointed out that the apparent ionic nature of a crystal such as KCl may in fact arise from the overlap of the potassium $4s$ electron's charge density onto the neighboring chlorine sites. According to this point of view, ionicity is the result of charge overlap rather than charge transfer. The present calculations involve crystal potentials formed from atomic charge densities containing a single metal $4s$ electron. Thus, these calculations effectively introduce some ionicity by means of these $4s$ overlap effects.

There is another effect which reduces the sensitivity of the energy-band results to the assumed degree of ionicity. This is the tendency for changes in the one electron energies that occur with increasing ionicity to be approximately cancelled by the Madelung contribution to the potential. To illustrate this cancellation, let us consider a simple example, namely TiO. The Herman-Skillman program[6] can be applied to calculate the ionic $3d$ one-electron energies for Ti^+ (d^3) and Ti^{2+} (d^2), the atomic $2p$ energy for O(p^4), and the ionic $2p$ energy for O^- (p^5). Since the program has difficulty with Ti(d^4) (which is barely bound) and O^{2-}(p^6) (which is not bound), we can estimate the corresponding orbital energies by linear extrapolation. If one takes the sum of these orbital energies and the appropriate Madelung potentials at the Ti and O nuclei, it is found that the p-d energy difference is constant to within ± 10% over the entire range of ionicities. Of course, this type of calculation only provides an order-of-magnitude estimate of this cancellation effect because it neglects the variation of the Madelung potential throughout the unit cell.

It is therefore suggested that there is little difference between the neutral-atom and ionic points of view. In the case of NiO, for example, either model predicts that the $3d$ bands contain eight electrons. However, the neutral-atom model assumes that oxygen $2s$-$2p$ bands contain sufficient admixture of nickel $3d$ and $4s$-$4p$ orbitals to maintain approximate charge neutrality within the unit cell.

In the present calculations, the exchange contribution to the crystal potential is treated according to Slater's original free-electron exchange approx-

imation.[9] It is expected that some features of the band structure would be modified if these calculations were performed self-consistently or if a different exchange approximation were introduced. Probably the most significant changes would correspond to shifts in the relative energies of the metal and oxygen bands. These shifts could be as large as a few electron volts.

B. LCAO Calculations

The LCAO interpolation method that is applied in this study involves a total of nine basis functions. These include five Bloch sums formed from transition-metal 3d orbitals as well as four similar functions formed from oxygen 2s and 2p orbitals. In the LCAO secular equation, it is assumed that the metal-metal and oxygen-oxygen orbital overlap integrals are small and can be neglected. More precisely, they are treated in the manner originally suggested by Slater and Koster.[4] However, the overlap between the metal 3d and oxygen 2s and 2p orbitals is included explicitly in the LCAO secular equation. For simplicity, the metal 4s-4p orbitals are omitted from this LCAO treatment. The results of Secs. III and IV indicate that s-d hybridization is fairly important, and the neglect of these hybridization effects limits the accuracy of this simplified LCAO model.

The detailed form of the LCAO Hamiltonian and overlap matrices for the sodium-chloride structure is summarized in Table II. The Hamiltonian matrix elements are expressed in terms of the energy integrals $E_{\alpha,\beta}(\vec{\mathbf{r}})$ of Slater and Koster.[4] However, the two-center approximation is applied in the actual fitting procedure. This two-center approximation reduces the total number of LCAO parameters from 26 to 16. Among these 16 two-center parameters, the oxygen-oxygen interactions are represented by a total of five parameters. These include the orbital energies E_s and E_p as well as the nearest-neighbor energy integrals $(ss\sigma)$, $(pp\sigma)$, and $(pp\pi)$. There are also a total of five d-d interaction parameters. Two of these are the e_g and t_{2g} orbital energies $E_{3z^2-r^2}$ and E_{xy}, respectively. In addition, there are the three nearest-neighbor energy integrals $(dd\sigma)$, $(dd\pi)$, and $(dd\sigma)$. Finally, the metal-oxygen interactions are represented by a total of six parameters. Three of these represent the energy integrals $(sd\sigma)$, $(pd\sigma)$, and $(pd\pi)$, while the last three (S_s, S_σ, S_π) represent the corresponding orbital overlap integrals.

C. Determination of LCAO Parameters

A systematic procedure has been developed for determining these LCAO parameters from the APW results at selected symmetry points in the Brillouin zone. This procedure is quite general, and with some modification, it can be applied to most crystal structures. In the present application, the APW

TABLE II. LCAO Hamiltonian and overlap matrix elements for the sodium-chloride structure, where $\xi = \frac{1}{2}k_x a$, $\eta = \frac{1}{2}k_y a$, and $\zeta = \frac{1}{2}k_z a$.

Basis functions

Type		No.	Origin
Ligand	s	1	$a(\frac{1}{2}, 0, 0)$
	x	2	$a(\frac{1}{2}, 0, 0)$
	y	3	$a(\frac{1}{2}, 0, 0)$
	z	4	$a(\frac{1}{2}, 0, 0)$
Metal	xy	5	(0, 0, 0)
	yz	6	(0, 0, 0)
	zx	7	(0, 0, 0)
	$3z^2-r^2$	8	(0, 0, 0)
	x^2-y^2	9	(0, 0, 0)

Ligand-ligand interactions

$$E_s \equiv E_{s,s}(000)$$
$$(ss\sigma) \equiv E_{s,s}(\tfrac{1}{2}\tfrac{1}{2}0)$$
$$E_p \equiv E_{x,x}(000)$$
$$P_1 \equiv E_{x,x}(\tfrac{1}{2}\tfrac{1}{2}0) = \tfrac{1}{2}(pp\sigma) + \tfrac{1}{2}(pp\pi)$$
$$P_2 \equiv E_{x,x}(0\tfrac{1}{2}\tfrac{1}{2}) = (pp\pi)$$
$$P_3 \equiv E_{x,y}(\tfrac{1}{2}\tfrac{1}{2}0) = \tfrac{1}{2}(pp\sigma) - \tfrac{1}{2}(pp\pi)$$
$$H_{1,1} = E_s + 4(ss\sigma)(\cos\xi\cos\eta + \cos\xi\cos\zeta + \cos\eta\cos\zeta)$$
$$H_{2,2} = E_p + 4P_1(\cos\xi\cos\eta + \cos\xi\cos\zeta) + 4P_2\cos\eta\cos\zeta$$
$$H_{3,3} = E_p + 4P_1(\cos\eta\cos\zeta + \cos\eta\cos\xi) + 4P_2\cos\zeta\cos\xi$$
$$H_{4,4} = E_p + 4P_1(\cos\zeta\cos\xi + \cos\zeta\cos\eta) + 4P_2\cos\xi\cos\eta$$
$$H_{2,3} = -4P_3\sin\xi\sin\eta$$
$$H_{3,4} = -4P_3\sin\eta\sin\zeta$$
$$H_{2,4} = -4P_3\sin\zeta\sin\xi$$

Metal-metal interactions

$$E_{xy} \equiv E_{xy,xy}(000)$$
$$D_1 \equiv E_{xy,xy}(\tfrac{1}{2}\tfrac{1}{2}0) = \tfrac{1}{4}[3(dd\sigma) + (dd\delta)]$$
$$D_2 \equiv E_{xy,xy}(0\tfrac{1}{2}\tfrac{1}{2}) = \tfrac{1}{2}[(dd\pi) + (dd\delta)]$$
$$D_3 \equiv E_{xy,xz}(0\tfrac{1}{2}\tfrac{1}{2}) = \tfrac{1}{2}[(dd\pi) - (dd\delta)]$$
$$E_{3z^2-r^2} \equiv E_{3z^2-r^2,3z^2-r^2}(000)$$
$$E_1 \equiv E_{3z^2-r^2,3z^2-r^2}(\tfrac{1}{2}\tfrac{1}{2}0) = \tfrac{1}{4}[(dd\sigma) + 3(dd\delta)]$$
$$E_2 \equiv E_{x^2-y^2,x^2-y^2}(\tfrac{1}{2}\tfrac{1}{2}0) = (dd\pi)$$
$$E_3 \equiv E_{xy,3z^2-r^2}(\tfrac{1}{2}\tfrac{1}{2}0) = -\sqrt{3}\,\tfrac{1}{4}[(dd\sigma) - (dd\delta)]$$
$$H_{5,5} = D_1 + 4D_2\cos\xi\cos\eta + 4D_3(\cos\xi\cos\zeta + \cos\eta\cos\zeta)$$
$$H_{6,6} = D_1 + 4D_2\cos\eta\cos\zeta + 4D_3(\cos\eta\cos\xi + \cos\zeta\cos\xi)$$
$$H_{7,7} = D_1 + 4D_2\cos\zeta\cos\xi + 4D_3(\cos\zeta\cos\eta + \cos\xi\cos\eta)$$
$$H_{8,8} = E_1 + E_2(4\cos\xi\cos\eta + \cos\xi\cos\zeta + \cos\eta\cos\zeta) + 3E_3(\cos\xi\cos\zeta + \cos\eta\cos\zeta)$$
$$H_{9,9} = E_1 + 3E_2(\cos\xi\cos\zeta + \cos\eta\cos\zeta) + E_3(4\cos\xi\cos\eta + \cos\xi\cos\zeta + \cos\eta\cos\zeta)$$
$$H_{5,6} = -4D_4\sin\zeta\sin\xi \qquad H_{6,9} = -2\sqrt{3}\,E_4\sin\eta\sin\zeta$$
$$H_{5,7} = -4D_4\sin\eta\sin\zeta \qquad H_{7,8} = 2E_4\sin\xi\sin\zeta$$
$$H_{5,8} = -4E_4\sin\xi\sin\eta \qquad H_{7,9} = 2\sqrt{3}\,E_4\sin\xi\sin\zeta$$
$$H_{6,7} = -4D_4\sin\xi\sin\eta \qquad H_{8,9} = \sqrt{3}(E_2 - E_3)(\cos\xi\cos\zeta + \cos\eta\cos\zeta)$$
$$H_{6,8} = 2E_4\sin\eta\sin\zeta$$

Metal-ligand interactions

$$(sd\sigma) \equiv E_{s,3z^2-r^2}(00\tfrac{1}{2}) \qquad S_s \equiv S_{s,3z^2-r^2}(00\tfrac{1}{2})$$
$$(pd\sigma) \equiv E_{z,3z^2-r^2}(00\tfrac{1}{2}) \qquad S_\sigma \equiv S_{z,3z^2-r^2}(00\tfrac{1}{2})$$
$$(pd\pi) \equiv E_{x,xy}(0\tfrac{1}{2}0) \qquad S_\pi \equiv S_{x,xy}(0\tfrac{1}{2}0)$$
$$H_{2,5} = 2i(pd\pi)\sin\eta \qquad S_{2,5} = 2iS_\pi\sin\eta$$
$$H_{3,5} = 2i(pd\pi)\sin\xi \qquad S_{3,5} = 2iS_\pi\sin\xi$$
$$H_{3,6} = 2i(pd\pi)\sin\zeta \qquad S_{3,6} = 2iS_\pi\sin\zeta$$
$$H_{4,6} = 2i(pd\pi)\sin\eta \qquad S_{4,6} = 2iS_\pi\sin\eta$$
$$H_{2,7} = 2i(pd\pi)\sin\zeta \qquad S_{2,7} = 2iS_\pi\sin\zeta$$
$$H_{4,7} = 2i(pd\pi)\sin\xi \qquad S_{4,7} = 2iS_\pi\sin\xi$$

TABLE II (*Continued*).

Metal-ligand interactions	
$H_{1,8}=(sd\sigma)(-\cos\xi-\cos\eta+2\cos\zeta)$	$S_{1,8}=S_s(-\cos\xi-\cos\eta+2\cos\zeta)$
$H_{1,9}=\sqrt{3}(sd\sigma)(\cos\xi-\cos\eta)$	$S_{1,9}=\sqrt{3}\,S_s(\cos\xi-\cos\eta)$
$H_{2,8}=-i(pd\sigma)\sin\xi$	$S_{2,8}=-iS_\sigma\sin\xi$
$H_{3,8}=-i(pd\sigma)\sin\eta$	$S_{3,8}=-iS_\sigma\sin\eta$
$H_{4,8}=2i(pd\sigma)\sin\zeta$	$S_{4,8}=2iS_\sigma\sin\zeta$
$H_{2,9}=\sqrt{3}\,i(pd\sigma)\sin\xi$	$S_{2,9}=\sqrt{3}\,iS_\sigma\sin\xi$
$H_{3,9}=-\sqrt{3}\,i(pd\sigma)\sin\eta$	$S_{3,9}=-\sqrt{3}\,iS_\sigma\sin\eta$

results for the transition-metal monoxides have been obtained at the symmetry points Γ, X, L, W, K, $\Delta(0,0,\frac{1}{2}\pi)$, and $\Sigma(\frac{1}{2}\pi,\frac{1}{2}\pi,0)$ in the Brillouin zone, where the coordinates in parentheses indicate the appropriate values for (ξ,η,ζ) in Table II.

In the first step of this procedure, the reduced Hamiltonian and overlap matrices are determined for the various irreducible representations at each of the symmetry points in the Brillouin zone where the APW bands are to be fitted. For the seven points listed above, this leads to a total of fifteen reduced 1 by 1 submatrices, ten 2 by 2 matrices, two 3 by 3 matricies, and two 4 by 4 matrices. This adds up to a total of 49 APW energy eigenvalues which are available to determine the 16 LCAO parameters. For the one-dimensional cases, the energy is a linear function of the LCAO parameters. In the remaining cases, the LCAO eigenvalues are nonlinear functions of these parameters.

The Taylor-series expansion method is used to solve this nonlinear least-squares fitting problem. In general terms, the problem is that of adjusting each of the ν LCAO parameters $P_1\cdots P_\nu$ to minimize D, the sum of the squares of residuals, where

$$D=\sum_{l=1}^{n}(E_l-\epsilon_l)^2\,, \tag{1}$$

and E_l and ϵ_l are the n APW and LCAO eigenvalues, respectively. If all the ϵ_l's were linear functions of the parameters P_j, the ν equations that result from setting $\partial D/\partial P_j=0$ for $j=1,\ \ldots\ \nu$ would be linear in P_j, and these equations could be solved numerically. However, when ϵ_l is a nonlinear function of the parameters P_j, an iterative procedure is required.

In the Taylor-series expansion method, a small correction δ_j is added to each parameter P_j. To lowest order, this leads to a system of equations that are linear in the corrections δ_j. One solves these linear equations to determine δ_j, adds these corrections to the original parameters P_j, and then repeats the procedure until D is a minimum. During each iteration (which is labeled by a superscript), one evaluates the n by ν matrix

$$Q_{ij}^s\equiv\Delta\epsilon_i^s/\Delta P_j^s\,, \tag{2}$$

whose elements are determined by successively incrementing each parameter and evaluating the change $\Delta\epsilon_i$ in the eigenvalue ϵ_i. The parameter increments have been chosen so that the largest energy change $\Delta\epsilon_i^s$ is between 0.001 and 0.01 Ry, which should minimize cancellation errors and higher-order effects. The linear equations for δ_j^s have the form

$$\underline{A}^s\,\underline{\delta}^s=\underline{B}^s\,, \tag{3}$$

where

$$A_{ij}^s=\sum_{l=1}^{n}Q_{li}^sQ_{lj}^s\,, \tag{4}$$

$$B_i^s=\sum_{l=1}^{n}Q_{li}^s(E_l-\epsilon_l^s)\,. \tag{5}$$

To avoid convergence difficulties, Hartley's method[10] of adding only a fraction of the correction δ_j^s to the parameters P_j^s has been applied. According to this method,

$$P_j^{s+1}=P_j^s+\alpha\delta_j^s\,, \tag{6}$$

where $0<\alpha\leq 1$. During each iteration cycle, the fraction α has been determined by evaluating D of Eq. (1) for $\alpha=0,\frac{1}{2}$, and 1, fitting the results with a parabola, and using interpolation to find the value of α that minimizes D.

Using these procedures, the LCAO parameters usually converge to values which are accurate to five or six decimal places within five or six iterations. Relatively crude order-of-magnitude estimates can be used to start the iteration procedure. The only cases in which the method failed to converge were those where the overlap matrices happened to become singular during an early iteration cycle. This situation occurred only when grossly unrealistic starting values were introduced to test the limitations of the method.

III. RESULTS

The APW energy-band results for the 3*d* transition-metal monoxides are summarized in Fig. 2, where $E(\vec{k})$ curves along the [100] or Δ direction are shown for the compounds CaO through NiO. For purposes of comparison, the zero of energy has been adjusted so it coincides with the top of the oxygen 2*p* bands, which has Γ_{15} symmetry in each case. The single band between -1.1 and -1.2 Ry originates from the oxygen 2*s* states. In CaO, the additional bands that appear near -1.0 Ry are due to the calcium 3*p* states. The unusual shape of these and the oxygen 2*s* bands suggests that substantial covalent mixing occurs between the oxygen 2*s* and calcium 3*p* orbitals, despite the fact that they are tightly bound core levels.

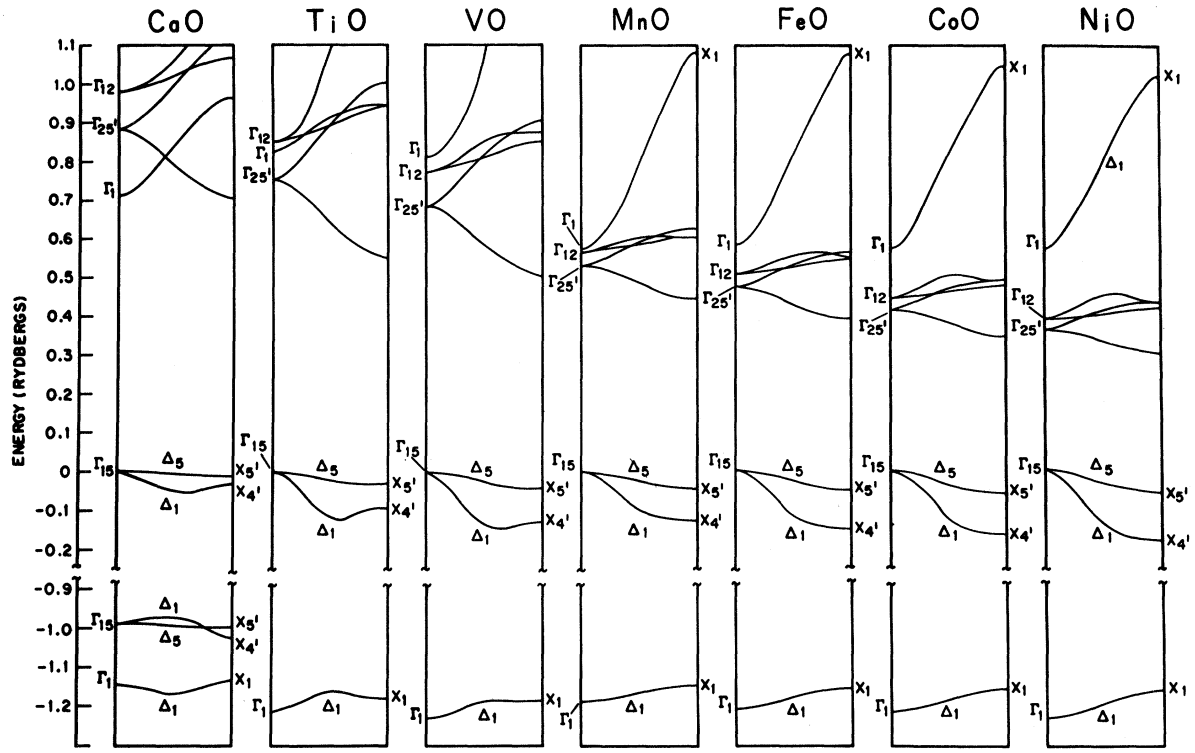

FIG. 2. APW energy-band results for the 3d transition-metal oxides plotted along the Δ direction of the Brillouin zone.

The remaining bands at positive energies correspond to the metal 3d and 4s-4p bands. The e_g and t_{2g} manifolds of the 3d bands originate from Γ_{12} and $\Gamma_{25'}$, respectively. The states with Γ_1 symmetry represent the bottom of the metal 4s-4p bands. Actually, these bands are more correctly described as antibonding metal-oxygen s-p bands.

To understand the variations in the band structure as the atomic number is increased, it is useful to consider first a slightly idealized system in which the lattice parameter is assumed to vary linearly from CaO to NiO. This is shown in Fig. 3. The observed lattice parameters for MnO, FeO, and CoO lie quite close to this line while those for TiO and VO are below it by about 10%. The interpolated lattice parameters for these hypothetical forms of TiO and VO would be 4.65 and 4.58 Å, rather than the observed values of 4.18 and 4.09 Å, respectively. For this idealized series of compounds, the energy of the Γ_1 state is approximately constant,[11] while the energy and width of the 3d band decreases continuously with increasing atomic number. These effects cause the 3d and 4s-4p bands to overlap in CaO and the metallic oxides TiO and VO. However, the 3d bands drop below Γ_1 in the antiferromagnetic insulators MnO to NiO.

Two changes occur in the band structures of TiO and VO when the lattice constants are decreased by 10% to the observed values.[11] First, the 3d bandwidth increases from 0.25 to 0.5 Ry. This change is caused not only by an increase in the strength of the direct d-d interactions, but also by the increased metal-oxygen interactions. Second, the reduced lattice parameter causes the 4s-4p band to

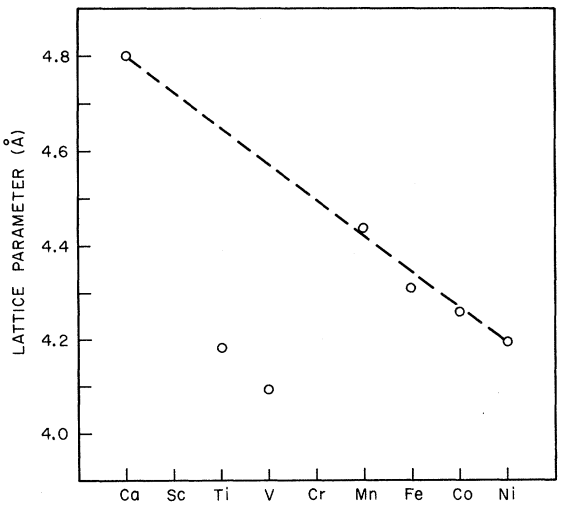

FIG. 3. Lattice parameters for the 3d transition-metal monoxides MO as a function of M.

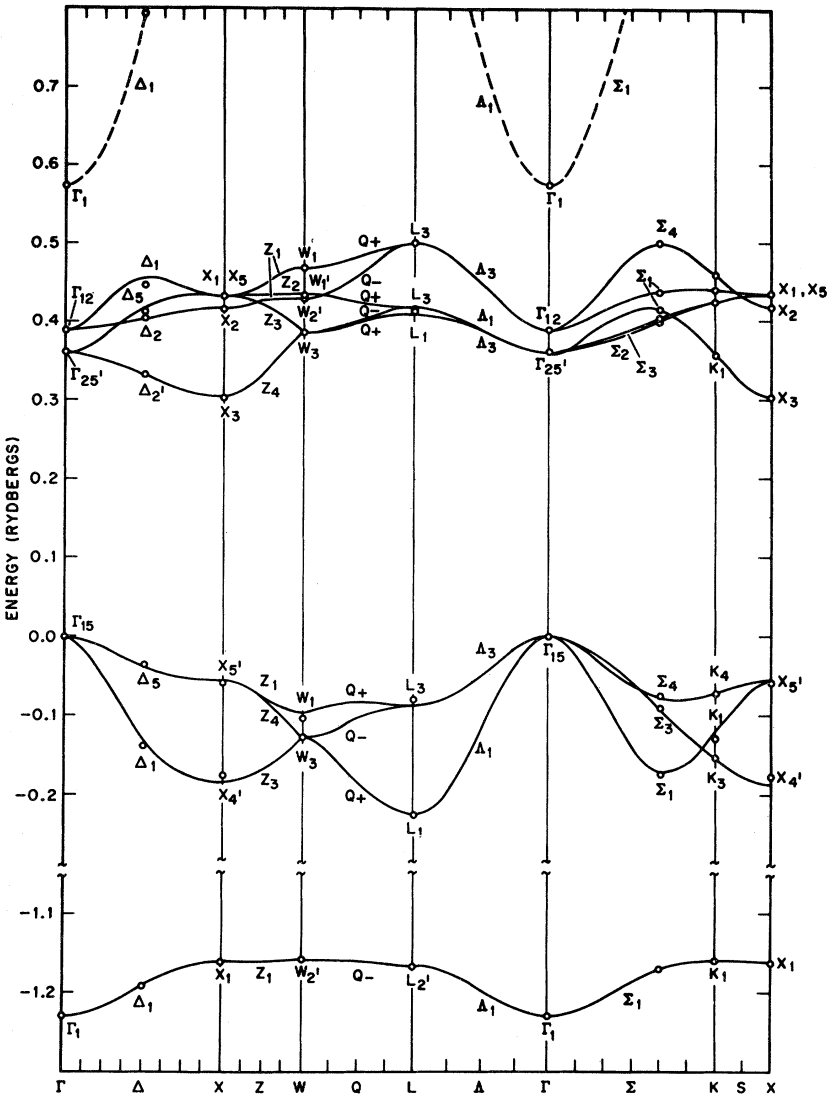

FIG. 4. LCAO energy bands for NiO obtained by fitting APW results at symmetry points.

be raised by about 0.2 Ry so that it no longer lies below the d bands at Γ. This change results from an increase in the overlap and covalency between the metal and oxygen s-p orbitals.

The APW results for the compounds TiO to NiO are listed in Table III. The last entry ΔE is the amount these results are shifted relative to the muffin-tin constant to set $E(\Gamma_{15})=0$. This is done prior to the LCAO fit. For comparison, this table also lists the LCAO eigenvalues that are obtained from the fitting procedure that is described in Sec. II. The 16 LCAO parameters for each of these compounds are listed in Table IV. The entries at the bottom of Table IV indicate the rms and maximum errors in each of these LCAO fits. It is found that the maximum error is usually associated with the 3d states which hybridize strongly with the metal 4s-4p bands, namely the states with Δ_1 symmetry. The gradual increase in the rms error from NiO to TiO partly reflects the increased importance of s-d hybridization. However, the increased 3d bandwidth indicates that the second-neighbor d-d interactions (which are omitted from the LCAO secular equation) could also contribute to this error, especially in TiO and VO.

A more complete picture of the NiO band structure is shown in Fig. 4, where $E(\vec{k})$ curves are plotted along the principal symmetry directions of the fcc Brillouin zone. The solid lines represent the LCAO bands for NiO, which are obtained using the LCAO parameters of Table IV. The open circles represent the APW results involved in the fitting procedure. The dashed curves indicate the lower portions of the nickel 4s-4p bands, which have been omitted from the LCAO matrix. The nickel 3d bands extend from L_3 and Σ_4 (which are nearly

TABLE III. APW results for the 3*d* transition-series monoxides and the LCAO fit to these results.

	TiO		VO		MnO		FeO		CoO		NiO	
	APW	LCAO	APW	LCAO	APW	LCAO	APW	LCAO	APW	LCAO	APW	LCAO
Γ_1	0.829	...	0.817	...	0.575	...	0.587	...	0.578	...	0.577	...
Γ_1	−1.205	−1.207	−1.228	−1.229	−1.186	−1.186	−1.205	−1.205	−1.215	−1.215	−1.229	−1.230
Γ_{15}	0.000	−0.001	0.000	0.000	0.000	−0.001	0.000	0.000	0.000	0.000	0.000	0.000
$\Gamma_{25'}$	0.753	0.741	0.683	0.672	0.530	0.525	0.475	0.470	0.418	0.414	0.365	0.361
Γ_{12}	0.855	0.849	0.773	0.770	0.569	0.568	0.511	0.510	0.448	0.448	0.392	0.391
Δ_1	1.095	...	1.068	...	0.789	...	0.804	...	0.795	...	0.797	...
Δ_1	0.912	0.965	0.856	0.892	0.603	0.624	0.559	0.574	0.501	0.511	0.449	0.457
Δ_1	−0.118	−0.111	−0.136	−0.128	−0.099	−0.094	−0.117	−0.111	−0.126	−0.119	−0.138	−0.131
Δ_1	−1.162	−1.163	−1.186	−1.186	−1.163	−1.162	−1.176	−1.175	−1.183	−1.181	−1.193	−1.191
Δ_2	0.898	0.896	0.812	0.810	0.588	0.586	0.528	0.527	0.464	0.463	0.406	0.405
$\Delta_{2'}$	0.645	0.642	0.585	0.583	0.488	0.486	0.436	0.434	0.385	0.383	0.335	0.334
Δ_5	0.896	0.895	0.814	0.817	0.591	0.592	0.534	0.537	0.471	0.475	0.415	0.419
Δ_5	−0.020	−0.024	−0.027	−0.031	−0.023	−0.025	−0.028	−0.031	−0.031	−0.034	−0.034	−0.038
X_1	...	...	...	...	1.080	...	1.077	...	1.040	...	1.014	...
X_1	0.947	0.942	0.875	0.872	0.603	0.602	0.553	0.552	0.491	0.490	0.436	0.435
X_1	−1.177	−1.177	−1.184	−1.185	−1.146	−1.147	−1.154	−1.154	−1.157	−1.157	−1.162	−1.162
X_2	0.942	0.944	0.850	0.851	0.604	0.605	0.544	0.544	0.477	0.478	0.418	0.418
X_3	0.558	0.543	0.504	0.495	0.447	0.446	0.396	0.397	0.350	0.352	0.304	0.307
$X_{4'}$	1.311	...	1.319	...	1.086	...	1.123	...	1.132	...	1.152	...
$X_{4'}$	−0.095	−0.109	−0.130	−0.143	−0.124	−0.131	−0.147	−0.156	−0.160	−0.169	−0.177	−0.186
X_5	1.002	0.993	0.902	0.896	0.627	0.626	0.566	0.565	0.497	0.497	0.436	0.436
$X_{5'}$	−0.029	−0.020	−0.040	−0.033	−0.040	−0.037	−0.048	−0.045	−0.052	−0.050	−0.058	−0.056
L_1	...	...	...	...	1.112	...	1.134	...	1.118	...	1.118	...
L_1	0.814	0.784	0.761	0.737	0.568	0.560	0.522	0.515	0.466	0.460	0.415	0.410
L_1	−0.182	−0.177	−0.212	−0.208	−0.163	−0.162	−0.192	−0.191	−0.207	−0.207	−0.227	−0.227
L_3	1.063	1.047	0.976	0.965	0.669	0.663	0.619	0.615	0.555	0.553	0.503	0.502
L_3	0.914	0.910	0.831	0.830	0.596	0.599	0.539	0.541	0.475	0.477	0.417	0.419
L_3	−0.089	−0.103	−0.097	−0.111	−0.055	−0.061	−0.066	−0.074	−0.071	−0.079	−0.079	−0.088
$L_{2'}$	1.110	...	1.090	...	0.900	...	0.914	...	0.911	...	0.915	...
$L_{2'}$	−1.104	−1.103	−1.137	−1.137	−1.144	−1.144	−1.153	−1.154	−1.158	−1.159	−1.166	−1.167
W_1	...	...	...	...	1.158	...	1.168	...	1.138	...	1.120	...
W_1	1.028	1.021	0.939	0.935	0.649	0.646	0.593	0.593	0.527	0.527	0.470	0.471
W_1	−0.095	−0.078	−0.107	−0.093	−0.074	−0.068	−0.087	−0.081	−0.095	−0.088	−0.104	−0.097
$W_{1'}$	1.002	0.993	0.902	0.896	0.627	0.626	0.566	0.565	0.496	0.497	0.435	0.436
$W_{2'}$	0.950	0.942	0.871	0.866	0.605	0.603	0.552	0.550	0.488	0.487	0.432	0.431
$W_{2'}$	−1.149	−1.149	−1.165	−1.164	−1.142	−1.142	−1.149	−1.150	−1.152	−1.153	−1.158	−1.158
W_3	...	...	...	...	1.194	...	1.215	...	1.210	...	1.218	...
W_3	0.769	0.795	0.709	0.726	0.547	0.552	0.497	0.499	0.441	0.441	0.390	0.388
W_3	−0.074	−0.078	−0.099	−0.102	−0.090	−0.090	−0.107	−0.107	−0.117	−0.117	−0.129	−0.129
Σ_1	1.235	...	1.202	...	0.924	...	0.933	...	0.926	...	0.930	...
Σ_1	0.945	0.960	0.867	0.875	0.610	0.613	0.557	0.558	0.494	0.494	0.438	0.439
Σ_1	0.862	0.863	0.797	0.796	0.584	0.585	0.532	0.533	0.470	0.471	0.415	0.416
Σ_1	−0.144	−0.135	−0.166	−0.159	−0.125	−0.121	−0.147	−0.143	−0.159	−0.155	−0.175	−0.170
Σ_1	−1.129	−1.129	−1.156	−1.155	−1.148	−1.148	−1.158	−1.158	−1.163	−1.163	−1.171	−1.171
Σ_2	0.882	0.885	0.799	0.798	0.584	0.582	0.526	0.523	0.462	0.459	0.405	0.402
Σ_3	...	...	...	...	1.274	...	1.290	...	1.281	...	1.284	...
Σ_3	0.783	0.806	0.725	0.746	0.556	0.562	0.507	0.513	0.451	0.457	0.401	0.405
Σ_3	−0.056	−0.067	−0.074	−0.082	−0.062	−0.064	−0.075	−0.076	−0.082	−0.083	−0.091	−0.092
Σ_4	1.054	1.042	0.972	0.964	0.668	0.663	0.619	0.615	0.555	0.552	0.503	0.499
Σ_4	−0.082	−0.086	−0.090	−0.094	−0.052	−0.054	−0.062	−0.065	−0.067	−0.070	−0.074	−0.078
K_1	...	...	...	...	1.227	...	1.240	...	1.227	...	1.228	...
K_1	...	...	...	...	1.137	...	1.145	...	1.115	...	1.096	...
K_1	0.966	0.959	0.889	0.884	0.614	0.612	0.563	0.561	0.499	0.498	0.444	0.442
K_1	0.675	0.689	0.620	0.632	0.505	0.509	0.456	0.459	0.405	0.407	0.357	0.358
K_1	−0.093	−0.083	−0.113	−0.104	−0.090	−0.085	−0.107	−0.101	−0.116	−0.110	−0.129	−0.121
K_1	−1.151	−1.151	−1.166	−1.166	−1.143	−1.143	−1.151	−1.151	−1.154	−1.154	−1.159	−1.159
K_2	0.968	0.965	0.873	0.870	0.615	0.615	0.555	0.554	0.487	0.486	0.427	0.426
K_3	...	...	...	...	1.135	...	1.163	...	1.164	...	1.178	...

TABLE III (*Continued*).

K_3	0.903	0.923	0.830	0.842	0.601	0.603	0.546	0.547	0.483	0.483	0.426	0.426
K_3	−0.086	−0.096	−0.116	−0.124	−0.106	−0.110	−0.127	−0.130	−0.138	−0.142	−0.153	−0.156
K_4	1.007	1.001	0.918	0.914	0.639	0.637	0.583	0.582	0.518	0.516	0.461	0.460
K_4	−0.059	−0.054	−0.070	−0.066	−0.050	−0.049	−0.060	−0.059	−0.065	−0.064	−0.072	−0.071
ΔE	−0.112		−0.145		0.053		0.012		0.003		−0.004	

degenerate) down to X_3, yielding a total bandwidth of 0.2 Ry. The oxygen $2p$ bands are slightly broader, having a width of 0.23 Ry.

The energy bands for CoO, FeO, and MnO are quite similar to those shown in Fig. 4 for NiO. Transversing this sequence of compounds, it is found that the $3d$ bandwidth increases by about 10% and the oxygen $2p$ bandwidth decreases by 30%. This increase in the $3d$ bandwidth is reflected in the LCAO parameters of Table IV by a corresponding increase in the $(dd\sigma)$, $(dd\pi)$, and $(dd\delta)$ integrals. This indicates that the linear increase in the lattice parameter does not quite compensate for the increase in the d-orbital radii that occurs as the atomic number is reduced.[6] However, this linear increase of the lattice parameter does cause a decrease in the $(pp\sigma)$ and $(pp\pi)$ integrals of Table IV, and this contributes to the narrowing of the $2p$ bands. The metal-oxygen overlap and covalency parameters S_s, $(sd\sigma)$, S_σ, $(pd\sigma)$, S_π, and $(pd\pi)$ remain constant to within 10% for each of these compounds.

The energy-band curves for TiO and VO are shown in Fig. 5. Again, the solid lines are the LCAO bands, the open circles represent the APW results, and the $4s$-$4p$ bands are dashed. The density-of-states curves shown at the right are calculated from the LCAO bands by sampling 55 296 uniformly distributed points in the fcc Brillouin zone. The Fermi energy for each compound is indicated by the dashed horizontal line. In each case, it falls about 0.02 Ry below Γ_1.

There is a noticeable decrease in the accuracy of the LCAO fit to the APW results. In the case of TiO, the LCAO bands predict that L_1 is below the Fermi level while the APW results place it above this energy. Thus, the LCAO bands would not represent the detailed Fermi-surface topology which is predicted by the APW results. These errors will also affect some details in the density-of-states curves. The importance of s-d hybridization is rather clear for the LCAO Δ_1 bands which originate from Γ_{12} since these fall 0.04 to 0.05 Ry above the APW results.

One surprising feature of the oxygen $2p$ bands is their width. Despite the fact that the lattice parameters for TiO and VO are smaller than those for NiO, the $2p$ bandwidths for TiO and VO are smaller than the corresponding width in NiO. This difference is not fully understood. At first sight, one is tempted to explain this decrease in the $2p$ bandwidth in terms of interactions involving the metal core states, since the titanium $3p$ bands are located about 0.4 Ry below the oxygen $2s$ band in

TABLE IV. Values for the tight-binding parameters that have been determined by fitting the APW results of Table III.

Parameter	TiO	VO	MnO	FeO	CoO	NiO
E_s	−1.1027	−1.1365	−1.1440	−1.1535	−1.1589	−1.1666
$(ss\sigma)$	−0.0086	−0.0077	−0.0035	−0.0043	−0.0047	−0.0053
E_p	−0.0370	−0.0525	−0.0515	−0.0616	−0.0674	−0.0743
$(pp\sigma)$	0.0179	0.0226	0.0199	0.0235	0.0255	0.0280
$(pp\pi)$	−0.0044	−0.0048	−0.0036	−0.0041	−0.0043	−0.0047
E_{xy}	0.8173	0.7399	0.5559	0.4995	0.4397	0.3849
$E_{3z^2-r^2}$	0.7785	0.7083	0.5410	0.4858	0.4280	0.3743
$(dd\sigma)$	−0.0569	−0.0511	−0.0229	−0.0215	−0.0186	−0.0167
$(dd\pi)$	0.0294	0.0255	0.0114	0.0103	0.0087	0.0076
$(dd\delta)$	−0.0047	−0.0033	−0.0015	−0.0012	−0.0009	−0.0008
S_s	0.0509	0.0561	0.0477	0.0469	0.0445	0.0427
$(sd\sigma)$	−0.1691	−0.1582	−0.0955	−0.0960	−0.0911	−0.0887
$S\sigma$	0.0858	0.0841	0.0645	0.0620	0.0566	0.0531
$(pd\sigma)$	−0.1235	−0.1215	−0.0737	−0.0774	−0.0761	−0.0762
S_π	−0.0256	−0.0327	−0.0317	−0.0330	−0.0317	−0.0305
$(pd\pi)$	0.0566	0.0555	0.0318	0.0342	0.0342	0.0349
rms error	0.0130	0.0095	0.0044	0.0038	0.0034	0.0035
max error	0.0534	0.0360	0.0207	0.0147	0.0106	0.0096

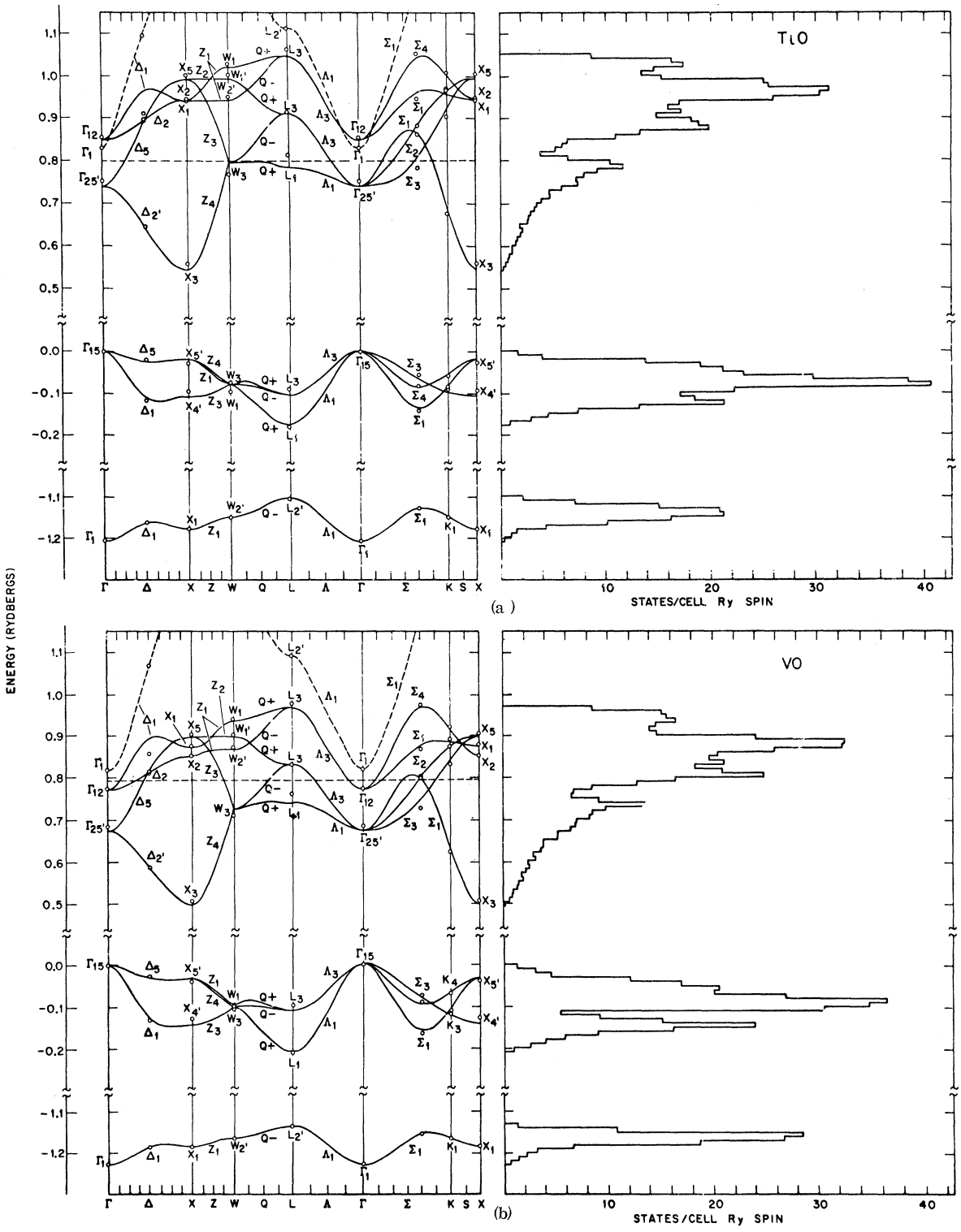

FIG. 5. (a) LCAO energy bands for TiO. (b) LCAO energy bands for VO.

Fig. 5. However, the total oxygen 2p bandwidth is determined by the state with L_1 symmetry, and this state does not interact with the titanium 3p bands. As a result, this explanation would have to involve the titanium 3s bands, which seems less likely since these levels are about -3.3 Ry on the energy

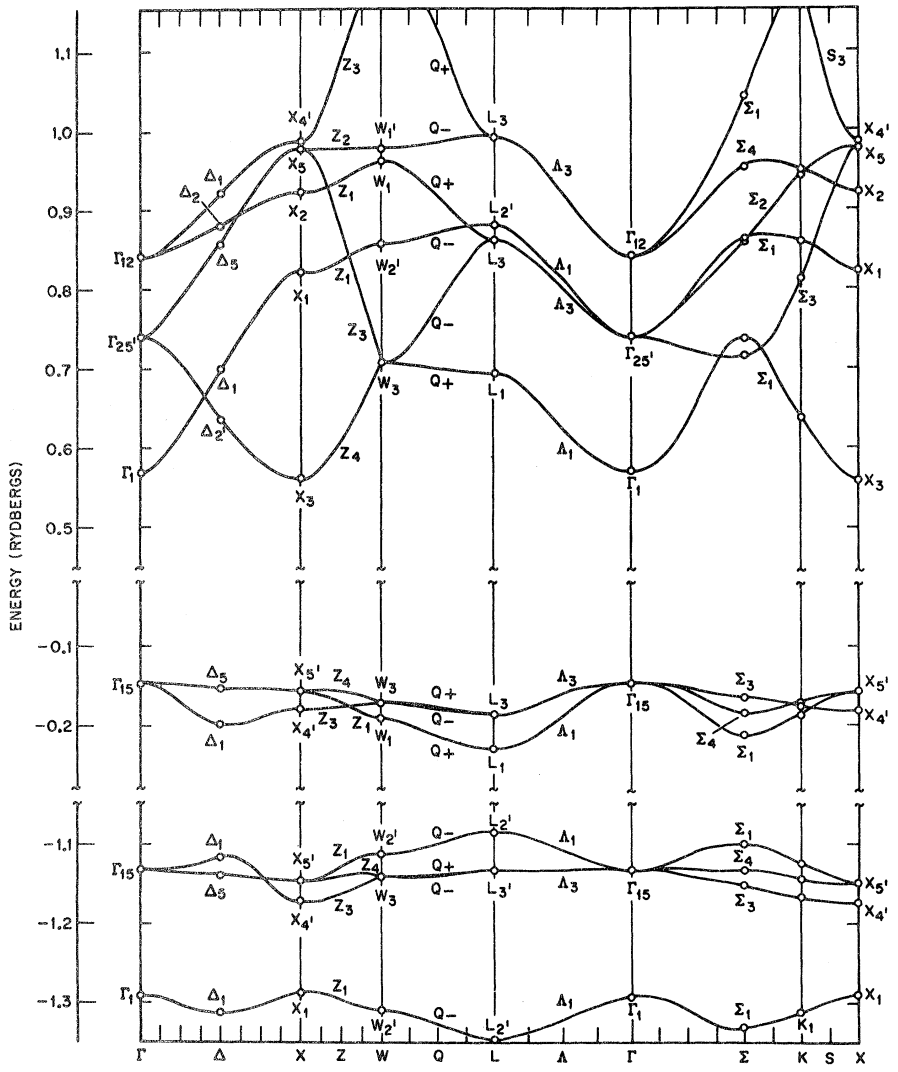

FIG. 6. APW energy-band results for CaO.

scale of Fig. 5.

The APW energy bands for CaO are shown in Fig. 6. The solid lines in this figure are only meant to indicate the general nature of the energy-band curves and are not obtained from an LCAO calculation. Clearly, such a calculation would require the addition of calcium $3p$, $4s$, and $4p$ orbitals to the restricted LCAO basis of Table II. Hybridization between the calcium $3d$ and $4s$-$4p$ bands produces significant changes in both sets of bands. The interaction between the calcium $3p$ and oxygen $2s$ bands is also quite obvious. The effect is particularly strong between the states with $L_{2'}$ symmetry. It is noted that $L_{2'}$ represents the bottom of the oxygen $2s$ band in CaO whereas it forms the top of this band in both TiO and VO. In the conduction bands, these calculations predict that Γ_1 and X_3 are nearly degenerate, but that X_3 has a slightly lower energy. These results predict an indirect $\Gamma_{15} \rightarrow X_3$ gap of 9.62 eV and direct gaps at Γ and X of 9.71 and 9.74 eV, respectively.

IV. DISCUSSION

The simplicity of the rocksalt structure permits one to isolate the various contributions to the $3d$ bandwidth in these compounds. This can be done qualitatively from the results shown in Figs. 2, and 4–6. For example, those states with Γ_{12}, $\Gamma_{25'}$, X_2, X_3, X_5, and $W_{1'}$ symmetry occur in the metal $3d$ but not the oxygen $2s$ or $2p$ bands. Therefore, that fraction of the $3d$ bandwidth spanned by these states is due to direct d-d interactions. The total width of the $3d$ band is further increased by metal-oxygen overlap and covalency effects. These additional contributions to the $3d$ bandwidth can be understood quantitatively by considering an effective Hamiltonian $\underline{H}'_{dd}$. This effective Hamiltonian contains not only the direct d-d interactions of Table II (metal-metal interactions) but also includes indirect terms (i.e., effective d-d interactions which

take place via the oxygen $2s$ and $2p$ orbitals).

It has been shown[5] that $\underline{H}'_{dd}$ has the form

$$\underline{H}'_{dd} = \underline{H}_{dd} + \Delta^{s}_{dd} + \Delta^{p}_{dd} \quad . \tag{7}$$

To second order, the last two terms on the right-hand side in Eq. (7) have the same wave-vector dependence as direct first- and second-neighbor d-d interactions. This combination of direct and indirect d-d interactions can be represented by introducing a set of effective energy integrals $\mathcal{E}_{\alpha,\beta}(\vec{r})$. These energy integrals replace the Slater-Koster integrals $E_{\alpha,\beta}(\vec{r})$ in d block of the LCAO matrix in Table II (metal-metal interactions). The relationship between the integrals $\mathcal{E}_{\alpha,\beta}(\vec{r})$ and $E_{\alpha,\beta}(\vec{r})$ for the rocksalt structure is indicated in Table V.

Each of the effective parameters $\mathcal{E}_{\alpha,\beta}(\vec{r})$ that is listed in the first column of this table contains a direct contribution $E_{\alpha,\beta}(\vec{r})$ and usually a second indirect term. The latter contribution is expressed in terms of the crystal-field parameters Δ_s, Δ_σ, and Δ_π that have been introduced previously in a study of crystal-field effects in the ReO_3 and perovskite structures.[5] These crystal-field parameters are determined from the LCAO parameters of Table IV by the relations

$$\begin{aligned}
\Delta_s &= 6\,[S_s E_{3z^2-r^2} - (sd\sigma)]^2/(E_{3z^2-r^2} - E_s)\ , \\
\Delta_\sigma &= 6\,[S_\sigma E_{3z^2-r^2} - (pd\sigma)]^2/(E_{3z^2-r^2} - E_p)\ , \\
\Delta_\pi &= 8\,[S_\pi E_{xy} - (pd\pi)]^2/(E_{xy} - E_p)\ .
\end{aligned} \tag{8}$$

It is obvious that each of these parameters is positive if the $3d$ bands are above the oxygen $2s$ and $2p$ bands. Assuming this is the case, the entries in the second column of Table V indicate whether the direct and indirect contributions add or cancel when they are added together to form the effective parameter $\mathcal{E}_{\alpha,\beta}(\vec{r})$. The entry in the third column indicates the angle θ between the vectors joining the intermediate oxygen with the two metal sites involved in the effective interaction. The one-center parameters $\mathcal{E}_{\alpha,\beta}(000)$ have $\theta = 0$; these represent the crystal-field effects of the ligand s-p orbitals on the metal d states. It has been shown[5] that the $10Dq$ splitting is equal to the difference between the average e_g and t_{2g} band energies, or $\mathcal{E}_{3z^2-r^2,3z^2-r^2}(000) - \mathcal{E}_{xy,xy}(000)$.

The nearest- and second-neighbor integrals have $\theta = 90°$ and $180°$, respectively. These integrals are responsible for the superexchange interactions which couple the spins on neighboring metal sites in the antiferromagnetic insulators.[2,5] It is interesting to note that the second-neighbor effective parameters for the rocksalt structure are identical with the nearest-neighbor parameters in the ReO_3 and perovskite structures.[5] In the ReO_3 and perovskite structures, the neighboring octahedral complexes share vertices along $\langle 100 \rangle$ and the nearest-neighbor metal-oxygen overlap and covalency interactions provide the superexchange mechanism for coupling the d electrons within these neighboring complexes. In the rocksalt structure, the neighboring octahedral complexes share edges along $\langle 110 \rangle$ and vertices along $\langle 100 \rangle$ and this leads to superexchange interactions in both directions. Undoubtedly these results can be extended to different stacking arrangements of octahedral complexes. The rutile structure, for example, contains slightly distorted octahedra which share edges along the c axis and vertices along the $\langle 110 \rangle$ directions in the basal plane. In the corundum structure, pairs of distorted octahedra share a common face along a unique threefold axis, while in the basal plane, the neighboring octahedra share edges. The results of Table V indicate that it should be possible to generalize this analysis of the effective d-d interactions so that it includes all three possibilities, namely vertex, edge, and face sharing between neighboring octahedral complexes.

The effective parameters $\mathcal{E}_{\alpha,\beta}(\vec{r})$ of Table V have been determined by fitting the APW results for the $3d$ band states of Table III with the eigenvalues of $\underline{H}'_{dd}$. The d block of the LCAO matrix is readily extended to include second-neighbor interactions from the tabulated results of Slater and Koster.[4] Using techniques similar to those described in Sec. II C, a total of 27 APW energy eigenvalues have been fitted to determine the 12 effective LCAO parameters of Table V. The values for these effec-

TABLE V. Contributions to the effective d-d LCAO interaction parameters

Effective parameter	Sum	θ	Contributions
$\mathcal{E}_{xy,xy}(000)$	add	0°	$E_{xy,xy}(000) + \frac{1}{2}\Delta_\pi$
$\mathcal{E}_{xy,xy}(\frac{1}{2}\frac{1}{2}0)$	...	...	$E_{xy,xy}(\frac{1}{2}\frac{1}{2}0)$
$\mathcal{E}_{xy,xy}(0\frac{1}{2}\frac{1}{2})$	...	...	$E_{xy,xy}(0\frac{1}{2}\frac{1}{2})$
$\mathcal{E}_{xy,xz}(0\frac{1}{2}\frac{1}{2})$	cancel	90°	$E_{xy,xz}(0\frac{1}{2}\frac{1}{2}) - \frac{1}{8}\Delta_\pi$
$\mathcal{E}_{xy,xy}(100)$	cancel	180°	$E_{xy,xy}(100) - \frac{1}{8}\Delta_\pi$
$\mathcal{E}_{xy,xy}(001)$	...	...	$E_{xy,xy}(001)$
$\mathcal{E}_{3z^2-r^2,3z^2-r^2}(000)$	add	0°	$E_{3z^2-r^2,3z^2-r^2}(000) + \frac{1}{2}(\Delta_s + \Delta_\sigma)$
$\mathcal{E}_{3z^2-r^2,3z^2-r^2}(\frac{1}{2}\frac{1}{2}0)$	cancel	90°	$E_{3z^2-r^2,3z^2-r^2}(\frac{1}{2}\frac{1}{2}0) + \frac{1}{12}\Delta_s$
$\mathcal{E}_{x^2-y^2,x^2-y^2}(\frac{1}{2}\frac{1}{2}0)$	cancel	90°	$E_{x^2-y^2,x^2-y^2}(\frac{1}{2}\frac{1}{2}0) - \frac{1}{4}\Delta_s$
$\mathcal{E}_{xy,3z^2-r^2}(\frac{1}{2}\frac{1}{2}0)$	...	...	$E_{xy,3z^2-r^2}(\frac{1}{2}\frac{1}{2}0)$
$\mathcal{E}_{3z^2-r^2,3z^2-r^2}(001)$	add	180°	$E_{3z^2-r^2,3z^2-r^2}(001) - \frac{1}{6}(\Delta_\sigma - \Delta_s)$
$\mathcal{E}_{x^2-y^2,x^2-y^2}(001)$	...	...	$E_{x^2-y^2,x^2-y^2}(001)$

TABLE VI. Effective d-d LCAO interaction parameters.

Parameter	TiO	VO	MnO	FeO	CoO	NiO
$\mathcal{E}_{xy,xy}(000)$	0.8420	0.7687	0.5707	0.5161	0.4556	0.4009
$\mathcal{E}_{xy,xy}(\frac{1}{2}\frac{1}{2}0)$	−0.0428	−0.0384	−0.0172	−0.0162	−0.0141	−0.0126
$\mathcal{E}_{xy,xy}(0\frac{1}{2}\frac{1}{2})$	0.0134	0.0119	0.0054	0.0049	0.0041	0.0036
$\mathcal{E}_{xy,xz}(0\frac{1}{2}\frac{1}{2})$	0.0092	0.0065	0.0027	0.0017	0.0008	0.0002
$\mathcal{E}_{xy,xy}(100)$	−0.0053	−0.0066	−0.0034	−0.0039	−0.0037	−0.0037
$\mathcal{E}_{xy,xy}(001)$	−0.0010	−0.0006	−0.0004	−0.0003	−0.0002	−0.0002
$\mathcal{E}_{3z^2-r^2,3z^2-r^2}(000)$	0.9827	0.9019	0.6284	0.5758	0.5123	0.4573
$\mathcal{E}_{3z^2-r^2,3z^2-r^2}(\frac{1}{2}\frac{1}{2}0)$	−0.0079	−0.0059	−0.0032	−0.0025	−0.0019	−0.0015
$\mathcal{E}_{x^2-y^2,x^2-y^2}(\frac{1}{2}\frac{1}{2}0)$	−0.0055	−0.0067	−0.0019	−0.0027	−0.0030	−0.0032
$\mathcal{E}_{xy,3z^2-r^2}(\frac{1}{2}\frac{1}{2}0)$	−0.0034	−0.0010	−0.0004	−0.0008	−0.0002	−0.0001
$\mathcal{E}_{3z^2-r^2,3z^2-r^2}(001)$	−0.0194	−0.0199	−0.0107	−0.0120	−0.0123	−0.0131
$\mathcal{E}_{x^2-y^2,x^2-y^2}(001)$	−0.0038	−0.0030	−0.0015	−0.0013	−0.0010	−0.0010
rms error	0.0162	0.0116	0.0054	0.0045	0.0039	0.0038
max error	0.0471	0.0337	0.0185	0.0151	0.0130	0.0121

tive parameters are listed in Table VI. For a given compound, the accuracy of this fit to the d-band states is comparable to that listed in Table IV. From the combined results of Tables II, IV–VI, one can easily determine the parameters Δ_s, Δ_σ, and Δ_π for each compound.

To illustrate the relative importance of the direct and indirect contributions to the energies of various d-band states, we consider the band structure of NiO. In Table VII, we list several states which occur once in the d band and also interact with the oxygen $2s$ and/or $2p$ band states. The entries under the "direct" heading are the band energies of each state if only the direct d-d interactions are considered, using the LCAO parameters of Table IV. The indirect contributions for each state are listed in the second column. These contributions involve the crystal-field parameters Δ_s, Δ_σ, and Δ_π in a manner that is indicated in the last column. The fourth and fifth columns compare the sum of the direct and indirect contributions with the exact LCAO results. The differences are due to the use of second-order perturbation theory to estimate the indirect terms. The results of Table VII demonstrate that the indirect contributions to the effective d-d interactions can be quite strong. They often shift energy eigenvalues by amounts which are comparable with the d bandwidth. It is clear that a simplified tight-binding calculation which includes the direct d-d interactions but neglects these indirect terms can be grossly in error.

The results of Table V illustrate another important point. Namely, while it is possible to treat the direct d-d interactions $E_{\alpha,\beta}(\vec{r})$ in the two-center approximation with reasonable accuracy, this approximation is not necessarily valid for the effective parameters $\mathcal{E}_{\alpha,\beta}(\vec{r})$. It turns out that the second-neighbor parameters can be expressed in terms of effective two-center integrals $(dd\sigma)_2'$, $(dd\pi)_2'$, and $(dd\delta)_2'$. These are related to the direct two-center integrals $(dd\sigma)_2$, $(dd\pi)_2$, and $(dd\delta)_2$ by the expressions

$$
\begin{aligned}
(dd\sigma)_2' &= (dd\sigma)_2 - \tfrac{1}{6}(\Delta_\sigma - \Delta_s)\ , \\
(dd\pi)_2' &= (dd\pi)_2 - \tfrac{1}{8}\Delta_\pi\ , \\
(dd\delta)_2' &= (dd\delta)_2\ .
\end{aligned}
\tag{9}
$$

However, the nearest-neighbor effective parameters $\mathcal{E}_{\alpha,\beta}(\frac{1}{2}\frac{1}{2}0)$ cannot be reduced to a comparable two-center form. If such a reduction is attempted, one obtains, for example, several expressions for $(dd\pi)'$ which involve $(dd\pi)$, but with different combinations of Δ_s, Δ_σ, and Δ_π.

It is enlightening to compare the energy-band results for the transition-metal monoxides with those for the fcc transition metals. A comparison between the energy bands for Ni and NiO is particularly useful in this respect. For this purpose, we can use the results of Zornberg,[12] who applied the combined interpolation method to fit the results of an APW calculation for nickel. Zornberg obtains a $3d$ bandwidth $[E(X_5) - E(X_3)]$ of about 0.3 Ry,

TABLE VII. Contributions of direct and indirect (i.e., via the oxygen orbitals) $d-d$ interactions to band energies for selected states in NiO, where $\Delta_s = 0.044$ Ry, $\Delta_\sigma = 0.122$ Ry, and $\Delta_\pi = 0.031$ Ry.

State	Direct	Indirect	Sum	LCAO	Indirect contribution
Δ_1	0.355	0.111	0.466	0.457	$\frac{2}{3}(\Delta_s+\Delta_\sigma)$
Δ_5	0.399	0.015	0.414	0.419	$\frac{1}{2}\Delta_\pi$
X_1	0.319	0.117	0.436	0.435	$\frac{8}{3}\Delta_s$
L_1	0.351	0.062	0.413	0.410	$2\Delta_\pi$
Σ_3	0.368	0.031	0.399	0.405	Δ_π
Σ_4	0.374	0.122	0.496	0.499	Δ_σ
W_1	0.393	0.081	0.474	0.471	$\frac{2}{3}\Delta_\sigma$
W_3	0.371	0.015	0.386	0.388	$\frac{1}{2}\Delta_\pi$
W_2'	0.344	0.088	0.432	0.431	$2\Delta_s$
K_3	0.410	0.015	0.425	0.426	$\frac{1}{2}\Delta_\pi$
K_4	0.399	0.061	0.460	0.460	$\frac{1}{2}\Delta_\sigma$

compared to the present width of 0.13 Ry for NiO. In metallic nickel, s-d hybridization increases the $3d$ bandwidth another 0.07 to 0.37 Ry. In NiO, covalency and overlap between the nickel $3d$ and oxygen $2s$-$2p$ orbitals also increase the $3d$ bandwidth by about 0.07 Ry, which leads a total bandwidth equal to 0.2 Ry.

These differences between the Ni and NiO $3d$ bandwidths are reflected in the relative magnitudes of the d-d interaction parameters. According to Zornberg, $(dd\sigma) = -0.038$ Ry, $(dd\pi) = 0.017$ Ry, and $(dd\delta) = -0.0017$ Ry. The results of Table IV indicate that these integrals in NiO are about half as large as those calculated for fcc nickel. This reduction is clearly due to the 20% increase in the nickel-nickel distance that occurs in the oxide.

The remaining differences in the energy bands for Ni and NiO are due to the strong "crystal-field effects", i.e., metal-ligand interactions that occur in the oxide but not the metal. In NiO, the states with L_3 and Σ_4 symmetry are nearly degenerate and form the top of the nickel $3d$ band. Both states are shifted to higher energies by the strong Δ_σ component of the crystal field. The states near the bottom of the $3d$ band in NiO are bonding with respect to d-d interactions and interact either weakly or not at all with the oxygen orbitals. The lowest state in the $3d$ band, X_3, falls into the latter category.

The energy difference $E(\Gamma_{12}) - E(\Gamma_{25}')$ in NiO is about one-third that found in fcc nickel. In the two-center approximation, this energy difference depends on $(dd\sigma)$, $(dd\pi)$, and $(dd\pi)$ as well as the difference

$$\gamma = E_{3z^2-r^2} - E_{xy} .$$

In fcc nickel, Zornberg finds that $\gamma \approx 0.0003$ Ry. The present results for NiO suggest that $\gamma = -0.01$ Ry. According to the LCAO model, γ involves two-center integrals between a d-orbital charge density at the origin and the atomiclike potentials of neighboring atoms. It is actually the difference between these terms for the e_g and t_{2g} orbitals, respectively. In fcc nickel, the largest contribution is due to the potentials of 12 neighboring nickel atoms at a distance of 2.5 Å. The t_{2g} orbital charge density overlaps these potentials more than the e_g orbitals, causes $E_{3z^2-r^2} > E_{xy}$, and leads to a positive γ. In a tight-binding calculation for nickel, Tyler *et al.*[13] calculate these integrals directly and find $\gamma = 0.0056$ Ry. The situation is reversed in the rock-salt structure. In NiO, the nearest potential to a nickel site is that of a neighboring oxygen atom at a distance of 2.1 Å along the ⟨100⟩ directions. This favors the e_g orbitals, causes $E_{3z^2-r^2} < E_{xy}$, and leads to negative values for γ.

While the values for γ in Table IV seem quite reasonable, they must be regarded as estimates to the actual values. For example, it has been found that if γ is set equal to zero and second-neighbor d-d interactions $(dd\sigma)_2$, $(dd\pi)_2$, and $(dd\delta)_2$ are included in the LCAO Hamiltonian, one obtains a slightly improved fit to the APW results and reasonable values for the second-neighbor integrals. Part of this improvement is due to the fact that two additional fitting parameters have been introduced. However, this result does indicate that second-neighbor d-d interactions are not completely negligible and that the present values for γ represent an upper limit to their actual values. If one attempts a similar calculation with $\gamma \neq 0$, then the LCAO fit to the APW results is again improved, but in this case the LCAO parameters converge to rather unrealistic values. This is attributed to the fact that this additional parameter γ over-determines the APW band structure at the seven points in the Brillouin zone where the LCAO fit is made. It is not clear whether this problem can be eliminated entirely if the fitting procedure is extended to include additional points in the Brillouin zone.

In view of this uncertainty in the magnitude of γ, it is important to compare the present values for γ with the values that have been determined directly in calculations involving the tight-binding method. In a recent tight-binding calculation for VO, Norwood and Fry[14] find $\gamma = -0.14$ Ry, which is substantially larger than the value of -0.032 Ry that is obtained for VO from the results of Table IV. In a molecular-orbital calculation for $KNiF_3$, Sugano and Shulman[15] find that $\gamma = -0.033$ Ry. This is larger than the value of -0.01 Ry that is obtained for NiO but comparable to the value for VO.

It is useful to compare some of the other LCAO parameters for VO with the corresponding tight-binding (TB) integrals of Norwood and Fry.[14] The results of such a comparison between the nearest- and second-neighbor d-d, s-d, and p-d LCAO parameters and TB integrals are contained in Table VIII. For convenience, the energy integrals $E_{\alpha,\beta}(\vec{r})$ of Norwood and Fry have been reduced to the two-center approximation. This leads to a range of values for the two-center integrals and these are enclosed within parentheses. The TB integrals that are presented in Table VIII correct some errors that occur in the paper by Norwood and Fry.[16] The LCAO parameters for VO from Table IV have been adjusted so that the TB and LCAO values for E_{xy} are equal. This involves a lowering of the LCAO energies by $\Delta E = -1.1347$ Ry. If the LCAO energy scale is shifted by an amount ΔE, then it has been shown[2,5] that each energy integral is changed by an amount equal to the product of the overlap integral and ΔE. The over-all differences between the LCAO parameters and the TB integrals suggest that the effective radii of the TB orbitals are somewhat larger than those for the corresponding LCAO orbitals, leading to energy and overlap

TABLE VIII. Comparison between the LCAO parameters and the tight-binding (TB) integrals of Norwood and Fry for VO. The zero of energy for the LCAO parameters has been shifted so that the LCAO and TB values for E_{xy} are equal.

	LCAO		TB	
	Energy (Ry)	Overlap	Energy (Ry)	Overlap
E_{xy}	−0.3948	1.0000	−0.3948	1.0000
$E_{3z^2-r^2}$	−0.4264	1.0000	−0.5347	1.0000
$(dd\sigma)_1$	−0.0511	0.0000	−(0.033, 0.048)	0.0362
$(dd\pi)_1$	0.0255	0.0000	(0.037, 0.071)	−0.0287
$(dd\delta)_1$	−0.0033	0.0000	−(0.012, 0.028)	0.0066
$(dd\sigma)_2$	0.0000	0.0000	−0.028	0.0087
$(dd\pi)_2$	0.0000	0.0000	0.010	−0.0048
$(dd\delta)_2$	0.0000	0.0000	−(0.001, 0.002)	0.0008
$(sd\sigma)_1$	−0.2219	0.0561	−0.3897	0.1212
$(sd\sigma)_2$	0.0000	0.0000	−0.0373	0.0123
$(pd\sigma)_1$	−0.2169	0.0841	−0.2889	0.1088
$(pd\sigma)_2$	0.0000	0.0000	−0.0369	0.0201
$(pd\pi)_1$	0.0926	−0.0327	0.1726	−0.0834
$(pd\pi)_2$	0.0000	0.0000	0.0191	−0.0073

integrals which are about twice as large as the LCAO parameters.

There have been a number of band-structure calculations for individual members of the 3*d* transition-metal-monoxide series involving either the APW or tight-binding methods. APW calculations have been carried out on TiO,[17,18] MnO,[19] and NiO,[19,20] while tight-binding results are available for TiO,[21] VO,[14] and NiO.[21] To avoid possible confusion, it is pointed out that the labelling of various states at the symmetry points L, Q, and W depends on the choice of the origin of coordinates. In the present calculation and in two of the previous ones,[14,21] the origin is at a metal-atom site. In the remaining calculations,[17,18,20] the origin is at an oxygen site. The latter choice interchanges the following representations: L_1 and $L_{2'}$; L_3 and $L_{3'}$; $Q+$ and $Q-$; W_1 and $W_{2'}$; $W_{1'}$ and W_2.

The APW results for TiO by Ern and Switendick[17] and Schoen and Denker[18] are quite similar to the present results. The main differences are in the calculated 3*d* bandwidths and the size of the energy gap which separates the 3*d* and 2*p* bands. Both previous calculations involve a partially ionic potential derived from Ti^+ and O^- charge densities. The calculation by Schoen and Denker includes the virtual-crystal approximation to estimate the effects of composition and vacancies on the electronic properties of TiO. The APW calculation by Switendick[20] for nonmagnetic NiO was the first application of this method to a compound. Switendick assumed a fully ionic model for the potential, and this led to a band structure in which the nickel 3*d* bands were below the oxygen 2*p* bands.

Wilson[19] has performed spin-polarized APW calculations for both MnO and NiO, thereby taking into account the effects of the magnetic superlattice. He finds that the 3*d* bands, which have a width of about 0.15 Ry, are split by intra-atomic exchange effects into two subbands. In MnO and NiO, this exchange splitting is about 0.4 and 0.3 Ry, respectively. In addition, Wilson finds that the magnetic superlattice further splits each of the 3*d* subbands into nonoverlapping e_g and t_{2g} manifolds. This model accounts for the insulating properties of MnO and NiO below their Néel temperatures. Wilson argues that these splittings will persist above the Néel temperature since they arise from intra-atomic rather than interatomic exchange interactions. Arguments will be presented in Paper II[2] which favor a localized rather than a band model for the antiferromagnetic insulators MnO to NiO. In a recent paper, Adler and Feinleib[22] also present semiempirical arguments for favoring a localized description of the 3*d* electrons in these materials.

The energy-band results for these transition-metal monoxides that have been obtained from tight-binding calculations appear to be less accurate. The calculations of Yamashita[21] for TiO and NiO neglect metal-oxygen interactions. In TiO, the 3*d* bandwidth of 0.46 Ry is fairly reasonable but the oxygen 2*p* bandwidth of 0.79 Ry is surprisingly large. In NiO, Yamashita finds the 3*d* bandwidth is reduced to 0.03 Ry while the 2*p* bandwidth remains close to the TiO value. The present results suggest that Yamashita's estimate of the 3*d* bandwidth in NiO is grossly underestimated. The tight-binding calculation of Norwood and Fry[14] for VO is more rigorous since it includes both two-and three-center integrals and sums over sufficient shells of neighboring atoms to achieve convergence in the Hamiltonian and overlap matrices. Unfortunately, this calculation contains some errors,[16] so that a detailed comparison with the present APW results for VO is not possible. Nevertheless, the results of Norwood and Fry do illustrate the important role that the oxygen 2*s* orbitals play in determining the nature of the VO conduction bands. A simplified calculation which includes only the vanadium 3*d* and oxygen 2*p* basis functions produces a band structure in which the bottom of the vanadium 4*s* band is far below the 3*d* bands. It is only when all the vanadium and oxygen core states are included in the secular equation that a band structure comparable to that shown in Fig. 5 is obtained.

This illustrates a common but important feature in the conduction bands of transition-metal compounds, namely, the fact that the bottom of the metal *s*-*p* band lies above rather than below the *d*-band states. It has been suggested[11] that this feature in the band structures of MnO to NiO is responsible

for the fact that the $3d$ electrons in these antiferromagnetic insulators are localized rather than itinerant.

It is a well-known fact that the s-p and d bands overlap in the transition metals so that both sets of bands are partially occupied. In the transition-metal compounds, the strong overlap and covalency interactions between the metal and ligand s-p orbitals raises the metal s-p bands so that they usually lie above the Fermi energy. The basic interactions that are responsible for this effect are quite analogous to the crystal-field effects which occur in the d bands. These effects can be described in terms of bonding and antibonding states formed from the metal and ligand s-p orbitals. According to this picture, the oxygen s-p bands in these monoxides represent bonding combinations of metal and oxygen s-p orbitals. The wave-vector dependence of the overlap and covalency interactions modulates the extent and nature of this bonding so that it varies throughout the Brillouin zone. From this point of view, the unoccupied metal s-p bands correspond to antibonding states with respect to metal-oxygen interactions. To second order, these s-p overlap and covalency effects shift the energy of the metal Γ_1 state by an amount

$$\Delta = 36\{SE_{4s} - [ss\sigma]\}^2/(E_{4s} - E_s)\ , \qquad (10)$$

where E_{4s} is the metal $4s$ orbital energy without the metal-oxygen interaction while $[ss\sigma]$ and S are the two-center metal-ligand energy and overlap integrals, respectively. Note that this shift Δ has the same form as the crystal-field parameters of Eq. (8). Its magnitude is increased by the larger numerical coefficient as well as the fact that the corresponding energy and overlap integrals $[ss\sigma]$ and S are larger for the metal s-p orbitals.

In ReO_3, it has been shown[5] that the bottom of the rhenium $6s$ band is shifted 0.6 Ry by these effects. In the LCAO approximation, the corresponding expression for Δ is one-third as large in the ReO_3 and perovskite structures. According to this model, the corresponding shift in the rocksalt structure would be 1.8 Ry for same overlap and covalency parameters. Taking into account the smaller radii of the $3d$ orbitals, it is estimated that $\Delta \approx 0.4$–0.5 Ry in the $3d$ monoxides.

One of the advantages of this combined APW-LCAO approach to the band structures of transition-metal compounds is that it provides a simple means for adjusting the energy-band results to obtain or improve the agreement between theory and experiment. It is expected that the main effects of self-consistency and improved treatments of exchange will be to alter the p-d band gap in these compounds.

TABLE IX. Comparison between the LCAO parameters for NiO that are obtained by lowering the $3d$ bands (E_{xy} and $E_{3z^2-r^2}$) by 0.179 Ry (LCAO shifted) and those determined directly from an APW calculation in which a constant of -0.2 Ry was added to the potential inside the nickel APW spheres (APW shifted).

Parameter	LCAO shifted	APW shifted
E_s	−1.1666	−1.1664
$(ss\sigma)$	−0.0053	−0.0056
E_p	−0.0743	−0.0787
$(pp\sigma)$	0.0280	0.0299
$(pp\pi)$	−0.0047	−0.0050
E_{xy}	0.2059	0.2045
$E_{3z^2-r^2}$	0.1953	0.1966
$(dd\sigma)$	−0.0167	−0.0139
$(dd\pi)$	0.0076	0.0055
$(dd\delta)$	−0.0008	−0.0003
S_s	0.0427	0.0368
$(sd\sigma)$	−0.0925	−0.0823
S_σ	0.0531	0.0447
$(pd\sigma)$	−0.0810	−0.0767
S_π	−0.0305	−0.0220
$(pd\pi)$	0.0376	0.0356

Therefore, it is useful to determine the accuracy with which the present LCAO model can predict the band structure of a material if the calculated band gap is varied by several electron volts. The results of such a determination are summarized in Table IX. To obtain these results, a separate APW calculation for NiO was carried out in which a constant potential of -0.2 Ry was added to the potential within the nickel APW spheres. This lowered the nickel $3d$ bands by about -0.18 Ry, thereby implying that 90% of the nickel $3d$ charge density is within the nickel spheres. The LCAO parameters that are determined from this APW calculation are listed under the heading "APW shifted" in Table IX. The corresponding "LCAO-shifted" parameters are obtained from those in Table IV by lowering E_{xy} and $E_{3z^2-r^2}$ for NiO by -0.179 Ry. In general, the agreement is quite good. However, the LCAO-shifted parameters fail to take into account the energy dependence of the d radial functions. As a result, the LCAO-shifted model predicts a $3d$ bandwidth which is 10% larger than the APW-shifted results. These results indicate that in terms of this simple LCAO model, one can modify the calculated band gap by as much as 50% and obtain bandwidths that are accurate to within about 10%.

ACKNOWLEDGMENT

I want to thank J. L. Fry for providing the various tight-binding integrals from his VO calculation that are referred to in this paper.

[1] D. Adler, in *Solid State Physics*, edited by F. Seitz, D. Turnbull, and H. Ehrenreich (Academic, New York, 1968).

[2] L. F. Mattheiss, following paper, Phys. Rev. B 5,

306 (1972).
[3]L. F. Mattheiss, Phys. Rev. 181, 987 (1969).
[4]J. C. Slater and G. F. Koster, Phys. Rev. 94, 1498 (1954).
[5]L. F. Mattheiss, Phys. Rev. B 2, 3918 (1970).
[6]F. Herman and S. Skillman, *Atomic Structure Calculations* (Prentice-Hall, Englewood Cliffs, N. J., 1963).
[7]P. D. DeCicco, Phys. Rev. 153, 931 (1967).
[8]J. C. Slater, *Quantum Theory of Molecules and Solids*, Vol. 2 (McGraw-Hill, New York, 1965).
[9]J. C. Slater, Phys. Rev. 81, 385 (1951).
[10]H. O. Hartley, Technometrics 3, 269 (1961).
[11]V. Heine and L. F. Mattheiss, J. Phys. C 4, L191 (1971).
[12]E. I. Zornberg, Phys. Rev. B 1, 244 (1970).
[13]J. M. Tyler, T. E. Norwood, and J. L. Fry, Phys. Rev. B 1, 297 (1970).
[14]T. E. Norwood and J. L. Fry, Phys. Rev. B 2, 472 (1970).
[15]S. Sugano and R. G. Shulman, Phys. Rev. 130, 517 (1963).
[16]J. L. Fry (private communication).
[17]V. Ern and A. C. Switendick, Phys. Rev. 137, A1927 (1965).
[18]J. M. Schoen and S. P. Denker, Phys. Rev. 184, 864 (1969).
[19]T. M. Wilson, Intern. J. Quantum Chem. 3, 757 (1970); J. Appl. Phys. 40, 1588 (1969).
[20]A. C. Switendick, Quarterly Progress Report, Solid-State and Molecular Theory Group, MIT, Vol. 49, p. 41, 1963 (unpublished).
[21]J. Yamashita, J. Phys. Soc. Japan 18, 1010 (1963).
[22]D. Adler and J. Feinleib, Phys. Rev. B 2, 3112 (1970).

PHYSICAL REVIEW B VOLUME 5, NUMBER 2 15 JANUARY 1972

Electronic Structure of the 3*d* Transition-Metal Monoxides. II. Interpretation

L. F. Mattheiss
Bell Laboratories, Murray Hill, New Jersey 07974
(Received 5 August 1971)

The results of augmented-plane-wave (APW) energy-band calculations for the 3*d* transition-series monoxides CaO, TiO, VO, MnO, FeO, CoO, and NiO are interpreted in terms of the electrical and optical data for these compounds. A detailed analysis of the effects of a crystalline field on the nonmagnetic *d* bands in the rocksalt structure shows that these bands are not split into nonoverlapping e_g and t_{2g} bands by a cubic field. Instead, these effects broaden the *d* bands in such a way that each of these compounds with partially filled *d* bands should exhibit metallic behavior. This model is consistent with the insulating properties of CaO and the metallic behavior of TiO and VO. However, the observed electrical and optical properties of MnO, FeO, CoO, and NiO suggest that these materials are Mott insulators, despite the fact that the present calculations predict 3*d* bandwidths $W \approx 3$ eV. Assuming that the 3*d* electrons in these materials are in localized Wannier rather than itinerant Bloch states, the APW energy bands are used to calculate the crystal-field parameters Δ for these insulating compounds, where Δ is the difference in the average energies of the e_g and t_{2g} bands. This leads to calculated values for Δ which are consistently 30% smaller than the experimental values. One interpretation of this discrepancy suggests that the true 3*d* bandwidths *W* are closer to 4 eV rather than 3 eV for these insulating compounds. Hubbard's simplified model calculations show that a Mott transition occurs when $W \approx U$, the Coulomb interaction energy between two electrons on the same atom. The fact that MnO to NiO are Mott insulators implies that $U > 4$ eV in these compounds.

I. INTRODUCTION

In the preceding paper[1] (hereafter referred to as I), the results of augmented-plane-wave (APW) energy-band calculations for the 3*d* transition-series monoxides CaO to NiO are presented. The purpose of the present paper is to interpret these energy-band results in terms of the electrical and optical data that is currently available for these compounds.

It has been found experimentally that these 3*d* transition-metal monoxides include materials with rather diverse and interesting physical properties. The series begins with CaO, which is a typical Bloch-Wilson insulator. Based on their reflectance measurements, Whited and Walker[2] estimate a band gap of 7 eV separating the oxygen 2*p* valence bands and the unoccupied calcium 3*d* and 4*s*-4*p* conduction bands. Strong exciton peaks obscure the actual band edge, and Van Vechten[3] has assigned a direct gap of 9.8 eV for this compound. However, the observation by Janin and Cotton[4] of a threshold for photoconductivity at 6.2 eV in powdered samples suggests a lower value for the band gap.

The next two members of this series, TiO and VO, exhibit metallic-type conductivity down to liquid-helium temperatures. There were early reports of a metal-insulator transition in VO near